Crossflow-Vortex Breakdown on Swept Wings: Correlation of Nonlinear Physics

R. D. Joslin and C. L. Streett

Theoretical Flow Physics Branch, Fluid Mechanics Division

NASA Langley Research Center, Hampton, Virginia 23681

ABSTRACT

The spatial evolution of crossflow-vortex packets in a laminar boundary layer on a swept wing are computed by the direct numerical simulation of the incompressible Navier-Stokes equations. A wall-normal velocity distribution of steady suction and blowing at the wing surface is used to generate a strip of equally spaced and periodic disturbances along the span. Three simulations are conducted to study the effect of initial amplitude on the disturbance evolution, to determine the role of traveling crossflow modes in transition, and to devise a correlation function to guide theories of transition prediction. In each simulation, the vortex packets first enter a chordwise region of linear independent growth, then, the individual packets coalesce downsteam and interact with adjacent packets, and, finally, the vortex packets nonlinearly interact to generate inflectional velocity profiles. As the initial amplitude of the disturbance is increased, the length of the evolution to breakdown decreases. For this pressure gradient, stationary modes dominate the disturbance evolution. A two-coefficient function was devised to correlate the simulation results. The coefficients, combined with a single simulation result, provide sufficient information to generate the evolution pattern for disturbances of any initial amplitude.

I. INTRODUCTION

Because of fierce competition and rising operational costs, the aircraft industry must utilize advanced technology in the design of the next generation of aircraft. One such technology is the reduction of external viscous drag (and fuel expenditures) by natural laminar flow control and by laminar flow control of the three-dimensional boundary-layer flow on the wings of the aircraft. The fuel savings translates directly into reduced operating costs in terms of millions of dollars over the life of a single aircraft.[1] Improvements in wing designs[2,3] and the implementation of devices such as suction for laminar flow control[4] and Gaster's bump[5] successfully reduce aircraft drag. These technological advances are successful because they are based on a fundamental understanding of three-dimensional boundary-layer flow physics. In the continued interest of drag reduction, the present paper documents both the effects of initial amplitudes on disturbance development and the role of traveling crossflow modes in transition. As the mechanisms of transition are better understood, the transition process can be more easily predicted and controlled. To this end, we have correlated the nonlinear instability information from the simulation results for future transition prediction.

The laminar boundary layer may be disturbed by factors such as surface irregularities, insect debris, and ice particles on the wing surface, combined with free-stream turbulence, noise, or vibrations. These factors influence the amplitudes and spectra of introduced instabilities.[6] Furthermore, the contamination that arises from wing and fuselage junctures can lead to transition close to the leading edge of the wing.[5] For extremely long-spanned aircraft, traveling waves may become unstable far from the fuselage and may cause transition on the outboard portion of the wings. Near the midchord regions of the wing, traveling waves can become unstable, and potential interactions with crossflow vortices already present in the boundary layer can cause transition. The chordwise location of the onset of this transition depends on the initial amplitudes of the disturbances.

Both stationary and traveling streamwise vortices (prior to transition) have been experimentally observed by Arnal, Coustols, and Juillen;[7] Poll;[8] Bippes and Nitschke-

Kowsky;[9] Müller and Bippes;[10] Dagenhart et al.;[11] and Dagenhart and Saric.[12] These instabilities are spawned from inflections in the mean velocity profile. Crossflow vortices are prevalent in regions of favorable pressure gradients (i.e., near the leading edge); traveling waves are suppressed in these regions. Identification of the instabilities that are of primary importance in the transition process at any chordwise location is a difficult task because both stationary and traveling modes are evolving in the flow.

Linear and secondary instability theories help determine dominant modes in the flow;[13,14,15] however, the lack of amplitude information and the inability to track multiple modes are deficiencies of theory. Furthermore, linearized theories cannot account for the potentially complex interactions in the disturbance field. Computational methods that solve the unsteady, nonparallel, nonlinear governing equations are the only tools available to identify the roles and relative importance of the various modes in the complex three-dimensional flow on the wing. Recently, Spalart,[16] with direct numerical simulations (DNS), and Malik and Li,[17] with parabolized stability equation (PSE) theory, have performed computational studies of crossflow disturbance evolution in swept Hiemenz flow.[18] Both the DNS and the PSE studies quantitatively agree and qualitatively capture the evolution of the disturbance up to the weakly nonlinear stage. Furthermore, Joslin and Streett[19] used DNS to identify three distinct stages in the breakdown process. They found that disturbances undergo stages of linear growth followed by vortex-vortex interactions and nonlinear vortex rollover. In the later stage, inflectional velocity profiles were observed; this observation is consistent with the experimental results of Dagenhart and Saric[12] and the computational results of Lin and Reed[20] and Fuciarelli and Reed.[21]

Here, the spatial evolution of nonlinear crossflow disturbances is computed by a simulation of the full Navier-Stokes equations (DNS). Choudhari and Streett[6] and Crouch[22] have shown with receptivity theory that free-stream noise, coupled with roughness elements on the wing surface, generates dominant stationary disturbances with amplitudes much larger than traveling modes. However, linear stability theory suggests that traveling modes should have larger growth rates; hence, these traveling modes should dominate.

3

Here, both stationary and traveling modes are introduced; the interaction and the mutual growth are computed. The initial disturbance amplitudes are varied, and the results are compared. Finally, the nonlinear simulation results are correlated to potentially guide later theories of transition prediction.

II. PROBLEM FORMULATION

To solve the problem numerically, the instantaneous velocities $\underline{\tilde{u}} = (\tilde{u}, \tilde{v}, \tilde{w})$ and the pressure $\tilde{p}$ are decomposed into base and disturbance components. The base flow is given by velocities $\underline{U} = (U, V, W)$ and the pressure P; the disturbance is given by velocities $\underline{u} = (u, v, w)$ and the pressure p. The velocities correspond to the coordinate system $\underline{x} = (x, y, z)$, where x is the chordwise direction, y is the wall-normal direction, and z is the spanwise direction. A sketch of the swept-wing problem is shown in figure 1. Note that the wing sweep direction corresponds to the positive z-direction and the direction of positive spanwise velocity. The computational domain is identified by region 2 of the figure. (Region 1 of the figure corresponds to the computational domain for the study of the attachment-line region.)

The base flow for the swept wedge is described by the Falkner-Skan-Cooke (FSC) similarity profiles.[23,24] To generate the velocity field, an analytical pressure gradient is imposed. This pressure matches the experimental results of Müller and Bippes[10] for their swept-wedge model.

For the disturbance portion of equation (1), the three-dimensional, incompressible Navier-Stokes equations are solved in disturbance form. These equations are given by

$$\frac{\partial u}{\partial t} + (\underline{u} \cdot \nabla)\underline{u} + (\underline{U} \cdot \nabla)\underline{u} + (\underline{u} \cdot \nabla)\underline{U} = -\Delta p + \frac{1}{R}\nabla^2 \underline{u} \tag{1}$$

with the continuity equation

$$\nabla \cdot \underline{u} = 0 \tag{2}$$

and boundary conditions

$$\underline{u} = 0 \quad \text{at} \quad y = 0 \quad \text{and} \quad \underline{u} \to 0 \quad \text{as} \quad y \to \infty \tag{3}$$

4

The Reynolds number $R = Q_R \delta / \nu$ is based on the boundary-layer thickness in the xy-plane defined as $\delta = \sqrt{\nu x_c / U_o}$ (where x_c is the chordwise coordinate normalized by the chord length) and local edge velocity $Q_R = Q_o$ at the computational inflow.

III. NUMERICAL METHODS

In this section, the numerical techniques required for the simulation and the disturbance forcing are briefly discussed. For a detailed description of the spatial DNS approach used for this study, refer to Joslin et al.[25,26]

The spatial discretization entails a Chebyshev-collocation grid in the wall-normal direction, fourth-order finite differences for the pressure equation, sixth-order compact differences for the momentum equations in the streamwise direction, and a Fourier series in the spanwise direction on a staggered grid.[26] For time marching, a time-splitting procedure is used with implicit Crank-Nicolson differencing for normal diffusion terms and an explicit three-stage Runge-Kutta method.[27] The influence-matrix technique is employed to solve the resulting pressure equation (Helmholtz-Neumann problem).[28,29] Disturbances are introduced into the boundary layer by suction and blowing techniques. At the inflow boundary, the mean base flow is forced, and at the outflow, the buffer-domain technique of Streett and Macaraeg[30] is used.

In this study, the vortex packets are forcibly imposed into the boundary layer by steady suction and blowing through the wedge surface in the same manner as described by Joslin and Streett.[19] Suction and blowing techniques may be used because, as demonstrated by Kachanov and Tararykin,[31] the results from suction and blowing and roughness-element disturbance generators correlate well and lead to disturbances that graphically coincide.

IV. RESULTS

For the simulations, no surface imperfections, particulates, weather-condition effects, noise, or spanwise inhomogeneities exist. Surface curvature is neglected to simplify the numerics and because the simulation is conducted on a chordwise region of the wing that corresponds to a relatively flat portion of a laminar flow airfoil.[11] The base flow and most

5

of the parameters used in the initial study by Joslin and Streett[19] are used here to enhance understanding of the transition process on swept wings.

The first simulation (SIM-I) is the case of Joslin and Streett.[19] This simulation has a grid of 901 streamwise, 61 wall-normal, and 32 spanwise grid points. The far-field boundary is located at 50δ from the wedge, the streamwise distance is 857δ from the inflow, and the spanwise distance is 108δ. For the time marching, a time-step size of $dt = 0.2$ is chosen for the three-stage Runge-Kutta method. For all simulations, crossflow-vortex packets are generated through a periodic strip of steady suction and blowing holes, equally spaced on the wing surface, and the shape of the wall-normal velocity profiles at the wall have a half-period sign wave in the chordwise direction and a full-period sine wave in the spanwise direction. Stationary crossflow-vortex packets are generated by steady suction and blowing with a wall-normal velocity component at the wall with an amplitude of $A = 1 \times 10^{-5}$. The holes for SIM-I have a chordwise length of 8.572δ and a spanwise length of 16.875δ.

The second simulation (SIM-II) has a grid of 501 streamwise, 61 wall-normal, and 64 spanwise grid points. The far-field boundary is located at 50δ from the wedge, the streamwise distance is 476δ, and the spanwise distance is 108δ. A time-step size of $dt = 0.4$ is chosen for time marching. Suction and blowing with the wall-normal velocity amplitude of $A = 1 \times 10^{-4}$ is used to generate the stationary and traveling crossflow vortices. The frequencies of twenty forced traveling modes range from $\omega = 0.6$ to $\omega = 1.2$. The holes for SIM-II have a chordwise length of 8.572δ and a spanwise length of 35.427δ.

The final simulation (SIM-III) has a grid of 421 streamwise, 61 wall-normal, and 64 spanwise grid points. The far-field boundary is located at 50δ from the wedge, the streamwise distance is 400δ, and the spanwise distance is 108δ. A time-step size of $dt = 0.4$ is chosen for time marching. The stationary and traveling crossflow-vortex packets are generated with both steady and unsteady suction and blowing with a wall-normal velocity component at the wall with an amplitude $A = 1 \times 10^{-3}$. The frequencies of twenty traveling modes range from $\omega = 0.6$ to $\omega = 1.2$. The holes for SIM-III have chordwise lengths of 8.572δ and spanwise lengths of 35.427δ.

As described in some detail by Joslin and Streett,[19] three distinct stages of disturbance evolution are expected. First, the growth of individual disturbance packets should be isolated from adjacent packets. Depending on the distance between the suction holes and the directions of the disturbance evolution, the individual packets should coalesce at some chordwise location downstream. If the vortex packets reach sufficiently large amplitudes in later stages of transition, then the disturbance field should be dominated by nonlinear interactions and vortex roll over. Each of the three simulations captures the different stages of this breakdown sequence. For example, figure 2 shows the contours of the logarithm of the disturbance vorticity for SIM-II as viewed from above the swept wedge. The different shades indicate the various levels of vorticity; two computational domains are shown side by side to describe the path of the disturbances generated from adjacent suction and blowing holes. Near the suction and blowing holes, the disturbance grows and spreads in the three-dimensional flow field in both the spanwise and the chordwise direction. A disturbance exits through the spanwise boundary (bottom of figure 2). Numerically, the disturbance reappears through the other spanwise boundary (top of figure 2) because periodicity is assumed; however, physically, the disturbance generated from an adjacent hole enters the domain, and its evolution is computed. At some chordwise location, vortex-vortex interactions begin to occur between adjacent vortices, and the amplitudes of the disturbances increase as denoted by the lighter contours. Figures 3–5 show spanwise slices (planes) of chordwise velocity contours viewed from the trailing edge toward the leading edge. (The wing tip is to the left, and the wing root is to the right.) For each simulation, the contour results show that immediately downstream of the disturbance initialization point a distinct vortex packet evolves that is isolated from nearby disturbances. As the disturbance evolves and spreads, vortices fill the span as a result of the vortex-vortex interactions or a spanwise instability mode. These vortex interactions lead to rapid increases in the disturbance growth rates, which in turn lead to disturbances that grow and interact nonlinearly. In this later, nonlinear stage of breakdown, the contours (figures 3–5) indicate that low-speed fluid is dragged out and over the high-speed fluid, which is drawn toward

7

the surface. Dagenhart and Saric[12] observed this same phenomenon in their experimental results, and Joslin and Streett[19] observed this phenomenon in their computations. So this breakdown sequence occurs regardless of the initial amplitudes of the disturbances; the initial amplitude apparently effects only the chordwise locations at which the stages begin.

In the nonlinear interaction region, inflectional velocity profiles are observed in all simulations. Figure 6 shows the instantaneous chordwise velocity profiles $(U + u)$ for each simulation at a chordwise station that corresponds to the nonlinear vortex rollover stage; the various profiles at each station correspond to adjacent spanwise locations. This vortex rollover stage cannot be described in detail by a linear method because of the inherent nonlinearity in the instabilities. Across the span, the flow is accelerated in regions near the wedge surface and is retarded in other areas out in the boundary layer. The characteristic inflectional profiles have been observed in experiments by both Müller and Bippes[10] and Dagenhart et al.,[11] and in computations by Lin and Reed,[20] Fuciarelli and Reed,[21] and Joslin and Streett.[19] Dagenhart et al.[11] noted that the appearance of inflectional profiles was rapidly followed by the appearance of a high-frequency instability and, subsequently, by transition. (No measurements were made in the experiments downstream of this stage.) The theoretical studies of Kohama et al.,[32] Reed and Fuciarelli,[33] and Balachandar et al.[15] it is clearly shown that this high-frequency instability in the experiments is reminiscent of secondary instabilities, which spawn from these inflectional velocity profiles. If a linear theory is to be used to predict transition, then it can only be used prior to this inflectional profile region. Furthermore, if laminar flow control is to be used to delay transition onset, then it must also be used prior to this rapid breakdown region.

The energy of the disturbances over the spanwise and wall-normal plane in the computational domain is shown with downstream location in figure 7. As outlined above and clearly shown in the figure, each simulation contains disturbances initiated with different amplitudes of suction and blowing and, subsequently, different energy levels. As the initial amplitudes of the disturbances become larger, the region of linear theory validity decreases, and the nonlinear vortex-interaction region encompasses the majority of the breakdown

region. If linear theories are to be used, then correlations are required in the nonlinear region. Here, the simulation data are correlated to enhance linear theory or future transition prediction theories.

Initially, a disturbance packet grows independently of other adjacent packets; exponential growth similar to that of primary instability modes is observed in this region. Downstream near the spanwise spreading region, an interruption in the exponential growth occurs, followed by a rapid increase in the disturbance growth rates. Joslin and Streett[19] showed that the computed disturbance followed the group-velocity path of linear stability theory until the vortex-interaction stage was reached. As a result, a linear theory alone is useless after this region of vortex-vortex interaction occurs because of the uncertainties in the propagation direction. However, this limitation of linear theory is true for any flow; once nonlinearities enter the flow, the linear theory is inadequate. However, the e^N method, which is based on linear stability theory, is a semiempirical approach that has been shown by Bushnell et al.[34] to predict transition for a broad class of flows. Normally, the e^N method results are presented in terms of logarithms of disturbance velocity, normalized by the initial amplitude. Simulation results in this form are shown in figure 8. The larger amplitude cases, which break down in much shorter chordwise distances, indicate N values of only 3 to 4; the small-amplitude case shows the expected $N \simeq 9$ value. (Note that the N corresponds to the exponential value in the e^N method and is equal to the ordinate of figure 8.) Correlation of the results with this normalizing definition indicates that as the initial amplitude of the disturbance increases the N value decreases significantly. This comparison is not useful in the theory because the transition point for each simulation case is depicted by different N values. Arguably, this prediction method should use normalizing amplitudes that correspond to branch I of the neutral curve; however, this information is unavailable in the simulations. If the smallest amplitude of SIM-I was used for all normalizing purposes, then figure 7 would result with a different ordinate scale. An alternate approach to predict transition involves the collapse of the simulation results onto one similarity-type curve with a correlation function.

This approach is not a new idea. Many years of research with these correlations have led to a better understanding of the turbulent boundary layer. (See Townsend.[35]) However, the correlation of both linear and nonlinear instabilities in a transitional boundary layer is a new approach. For the following database of crossflow breakdown results, correlations of the linear growth region of the instabilities (shown in figure 7) is examined. After many numerical experiments, the correlation results shown in figure 9 were obtained with the following two-coefficient function:

$$x_{cor} = x_r + (x_c - x_r) \times e^{c_1} \tag{4a}$$

$$E_{cor} = E/E_r \times 10^{(x_c - x_r)/x_r)c_2} \tag{4b}$$

where the subscript r denotes reference conditions and c_1 and c_2 are the correlation coefficients, both of which are discussed in more detail later in the text. As seen in figure 9, the linear growth regions of the individual simulations correlate well with this functional representation. The curves begin to deviate slightly at the region of vortex-vortex interactions and throughout the nonlinear region. This deviation in the nonlinear region is not unexpected because obvious differences exist in this region (shown in figure 7). Because these simulations are essentially noise free, the necessary frequency spectra required to achieve transition are absent from the computations. Without these unsteady components, the stationary crossflow components can grow without bound and without triggering transition. As a result, the peak amplitudes of the crossflow results are only important to indicate that both the disturbance levels and the physics are comparable to those observed in the experiments. The peak amplitude levels can signal when the important vortex-rollover phenomenon is dominant and, in the absence of transition in the computations, can serve as the artificial point of transition for discussion.

The coefficients of equation (4), which are used to generate figure 9, are determined such that the linear growth region correlates. The resulting coefficients are $c_1 = \{0, 0.38, 0.58\}$ and $c_2 = \{0, 4.5, 8.0\}$, which correspond to the simulations {SIM-I, SIM-II, SIM-III}. Figure 10 shows the interpolated coefficients with initial disturbance

amplitudes. The coefficient c_1 indicates a nearly linear variation with initial disturbance amplitude; c_2 is nearly linear for small amplitudes, but increases more rapidly than the initial disturbance amplitude for large amplitudes. If the coefficients and amplitudes in figure 10 are used with one reference simulation (SIM-I), then the evolution pattern of a disturbance with any initial amplitude is known from the correlation function in equation (4). To demonstrate, figure 11 shows the evolution of many disturbances with chordwise position. A comparison of the correlated results with the SIM-II and SIM-III results reveals good quantitative agreement in the linear growth region and indicates expected differences in the nonlinear region; however, the essential qualitative features in the nonlinear region are captured by the correlation function. The second comparison in figure 11 shows the effect of initial amplitude on both the extent of linear growth and the location of peak amplitude (transition). The correlated data demonstrates how the transition point moves upstream as the initial amplitude increases.

This discussion of correlation functions leaves many questions unanswered (e.g., how the coefficients vary with Reynolds number and angle of attack); however, it does provide an initial starting point for the derivation of better and more complete relations. Furthermore, many different instabilities and variations in computational parameters (e.g., grids) were introduced in these simulations. Figures 2–6 indicate that in spite of this variation the dominate physics of the flow have been captured in all of the simulations. However, additional simulations are necessary to adequately fine-tune the correlation tool and to determine the universality of the coefficients.

The role of stationary and traveling modes will be addressed in the remainder of this section. As mentioned at the beginning of this section, both stationary and traveling modes were excited in SIM-II and SIM-III; however, no differentiation between the different modes has explicitly been made in this paper. Furthermore, the correlation functions were derived without reference to the unsteady components present in the flow. In the remainder of this paper, we show that the above comparisons remain valid because the stationary (steady) mode is dominant in comparison with the unsteady modes.

11

To determine the individually dominant modes, the spectra are obtained from each simulation by a Fourier series analyzer. Because periodicity is assumed in the spanwise direction, Fourier series are appropriate; however, a window of temporal data must be assumed (similar to experimental techniques) to use Fourier series in time. The frequency and spanwise wavenumber spectra can be examined to determine the dominant modes which are evident by the large energy contents. Figure 12 shows the most dominant modes with the frequency and spanwise wave-number spectra in the nonlinear vortex rollover region of breakdown. Here, the dominant mode has a frequency of zero in all simulations and the energy levels rapidly decay (drop off) in the unsteady modes. In the experiments, secondary instability modes were observed in this region; however, the simulation results indicate that no high-frequency modes occur. The absence of high-frequency modes suggests that the inflectional profiles arise from the stationary crossflow modes alone and that the simulations are virtually free from the noise sources that generate the important unsteady modes. Although unsteady modes were forced in both SIM-II and SIM-III, the proper modes that lead to high-frequency modes were not found in the simulations. Figure 13 shows profiles of the stationary crossflow modes with spanwise wave numbers, and figure 14 shows profiles of the dominant stationary crossflow modes as they evolve along the wing chord. Figure 13 indicates that in this later stage of breakdown, significant energy can be found in the harmonics, but the flow is resolved with the grids that are used in the simulations. The mean-flow distortion component has sufficient energy to alter the mean flow (see figure 6), which further indicates nonlinear activity in this region. In figure 14, the profiles early in the simulation take on shapes that can be described by linear theory. (See Fuciarelli and Reed.[21]) As the disturbance amplitudes increase with downstream distance, nonlinear interactions lead to profiles that have two peaks (shown clearly in the SIM-I results). This double-peak feature in the nonlinear regime agrees with the experiments of Dagenhart and Saric[11] and further indicates the inadequacy of linear theory for this stage of breakdown.

V. CONCLUDING REMARKS

The spatial evolution of crossflow-vortex packets in a laminar boundary layer on a swept wing were computed by direct numerical simulation of the incompressible Navier-Stokes equations. Three distinct and subsequent stages of disturbance evolution were observed in all simulations; these results agree with the previous study by Joslin and Streett.[19] A disturbance that is ingested into the flow will eventually interact nonlinearly and lead to inflectional profiles; these inflectional profiles are observed experimentally just prior to the laminar-to-turbulent transition location. The characteristic inflectional profiles have been observed in experiments by both Müller and Bippes[10] and Dagenhart et al.,[11] and in computations by Lin and Reed,[20] Fuciarelli and Reed,[21] and Joslin and Streett.[19]

Dagenhart et al.[11] noted that the stationary crossflow disturbance dominates the instabilities present in the flow until the inflectional profiles develop; this development of inflectional profiles results in an explosive growth of secondary instability modes, which in turn leads to transition. Müller and Bippes[15] argue that traveling modes are more important in the transition process; however, they suggest that the inflectional profiles, deformed by stationary vortices, lead to the growth of secondary instabilities. The present computational study of stationary and traveling crossflow disturbances indicates that stationary modes are dominant in the boundary layer at this angle of attack, Reynolds number, and base flow and that the growth of stationary modes causes instantaneous inflections in the velocity field. Although unsteady modes were forced, no secondary instability modes were excited in the vortex rollover region.

A two-coefficient correlation function was introduced to combine the evolution pattern of disturbances generated with different initial amplitudes. These preliminary results indicate that the correlations can be made and can potentially provide a database to test theories of transition prediction at low computational cost.

REFERENCES

[1] F. S. Collier Jr., (personal communication), August 1993.

[2] J. K. Viken, R. L. Campbell, S. A. W. Viken, W. Pfenninger, H. L. and Morgan, *Natural Laminar Flow and Laminar Flow Control Symposium*, NASA Langley Research Center, Hampton, VA (1987).

[3] G. S. Manuel and W. A. Doty, AIAA Paper No. 90-1310 (1990).

[4] D. V. Maddalon, F. S. Collier Jr., L. C. Montoya, and C. K. Land, AIAA Paper No. 89-1893 (1989).

[5] M. Gaster, *J. Roy. Aero. Soc.* **69**, 788 (1965).

[6] M. Choudhari and C. L. Streett, HTC Rep. No. HTC-9301 (1993).

[7] D. Arnal, E. Coustols, and J. C. Juillen, *Rech Aérosp No. 1984-4* p. 39, (1984).

[8] D. I. A. Poll, *J. Fluid Mech.* **150**, 329 (1985).

[9] H. Bippes and P. Nitschke-Kowsky, AIAA Paper No. 87-1336 (1987).

[10] B. Müller and H. Bippes, AGARD-CP-438 (1988).

[11] J. R. Dagenhart, W. S. Saric, M. C. Mousseux, and J. P. Stack, AIAA Paper No. 89-1892 (1989).

[12] J. R. Dagenhart and W. S. Saric, Submitted to *AIAA J.*, (1993).

[13] U. Dallman and H. Bieler, AIAA Paper No. 87-1337 (1987).

[14] T. M. Fischer and U. Dallmann, AGARD-CP-438 (1988).

[15] S. Balachandar, C. L. Streett, and M. R. Malik, AIAA Paper No. 90-1527 (1990).

[16] P. R. Spalart, *Laminar-Turbulent Transition*, (D. Arnal and R. Michel, eds.), (Springer-Verlag, Berlin Heidelberg, 1990).

[17] M. R. Malik and F. Li, *Aerotech '92*, Paper No. 921991 (1992).

[18] P. Hall, M. R. Malik, and D. I. A. Poll, *Proc. Roy. Soc. Lond.* **A 395**, 229 (1984).

[19] R. D. Joslin and C. L. Streett, Submitted to *Phys. Fluids A* (1993).

[20] R.-S. Lin and H. L. Reed, Submitted to *Phys. Fluids A*, (1993).

[21] D. A. Fuciarelli and H. L. Reed, *Phys. Fluids A* **4**(9), 1880 (1992).

[22] J. D. Crouch, AIAA Paper No. 93-0074, (1993).

[23] J. C. Cooke, *Proc. Camb. Phil. Soc.* **46**, 645 (1950).

[24] V. M. Falkner and S. W. Skan, *Phil. Mag.* **12**, 865 (1931).

[25] R. D. Joslin, C. L. Streett, and C.-L. Chang, NASA TP-3205, (1992).

[26] R. D. Joslin, C. L. Streett, and C.-L. Chang, *Theor. & Comput. Fluid Dyn.* **4**(6), 271 (1993).

[27] J. H. Williamson, *J. Comp. Phys.* **35**(1), 48 (1980).

[28] C. L. Streett and M. Y. Hussaini, *Appl. Numer. Math.* **7**, 41 (1991).

[29] G. Danabasoglu, S. Biringen, and C. L. Streett, *Phys. Fluids A* **3**(9), 2138 (1991).

[30] C. L. Streett and M. G. Macaraeg, *Int. J. Appl. Numer. Math.* **6**, 123 (1989).

[31] Y. S. Kachanov and O. I. Tararykin, *Laminar-Turbulent Transition*, (D. Arnal and R. Michel, eds.), (Springer-Verlag, Berlin Heidelberg, 1990).

[32] Y. Kohama, W. S. Saric, and J. A. Hoos, *Proc. R. Aeronaut. Soc. Conf. on Boundary-Layer Transition and Control*, Cambridge University (1991).

[33] H. L. Reed and D. A. Fuciarelli, *Bull. Amer. Phys. Soc.* **36** (10), 2630 (1990).

[34] D. M. Bushnell, M. R. Malik, and W. D. Harvey, *IUTAM Symposium*, (J. Zierep and H. Oertel, eds.), (Springer-Verlag: Berlin, 1988).

[35] A. A. Townsend, *The Structure of Turbulent Shear Flow*, (Cambridge U. P., Cambridge, England, 1976).
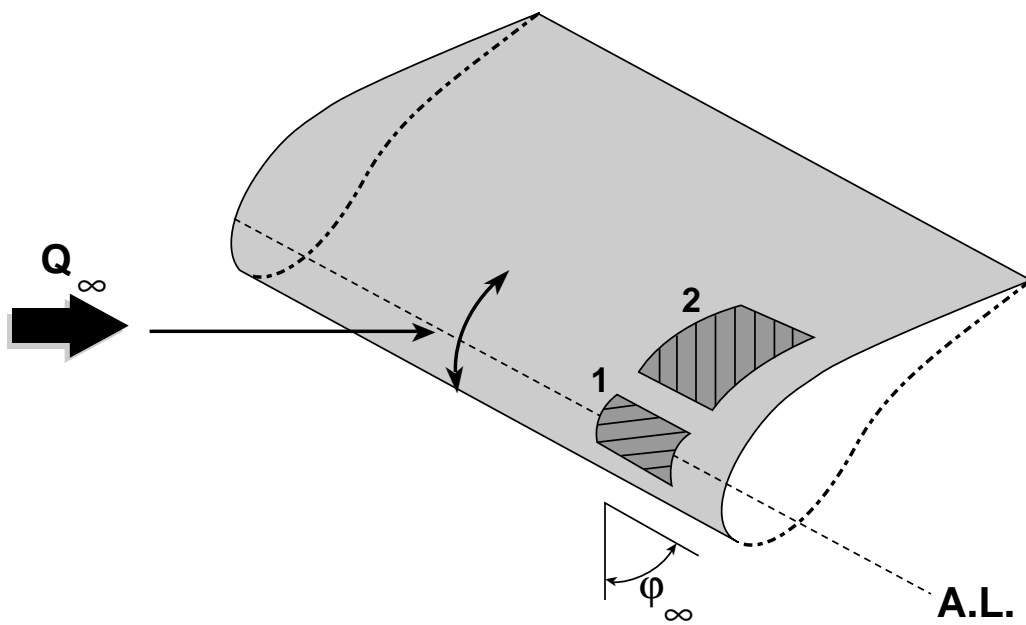
Figure 1. Sketch of swept-wing (1) attachment-line region and (2) laminar-to-turbulent transition region.
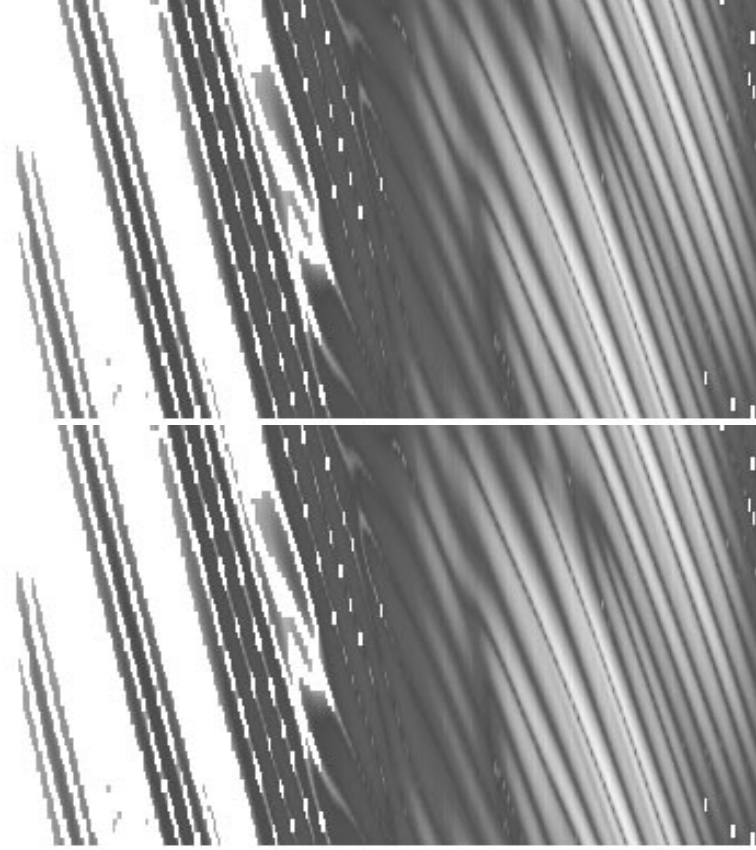
Figure 2. Top view of disturbance vorticity (log Ω) contours for simulation SIM-II for swept-wedge flow.

(a) $x_c = 0.25$
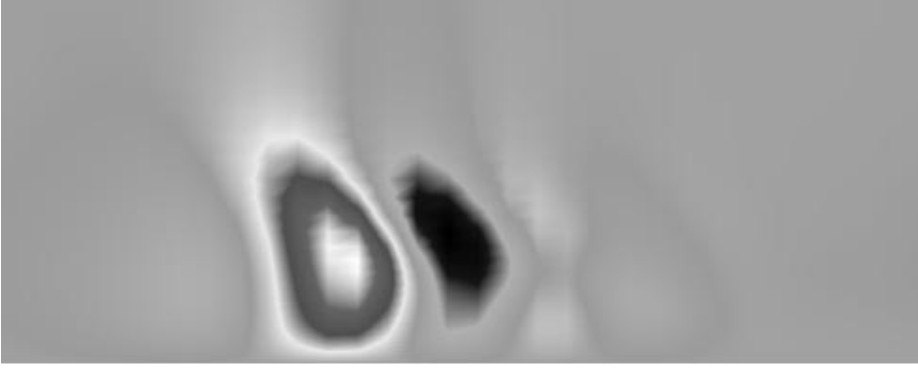
(b) $x_c = 0.34$
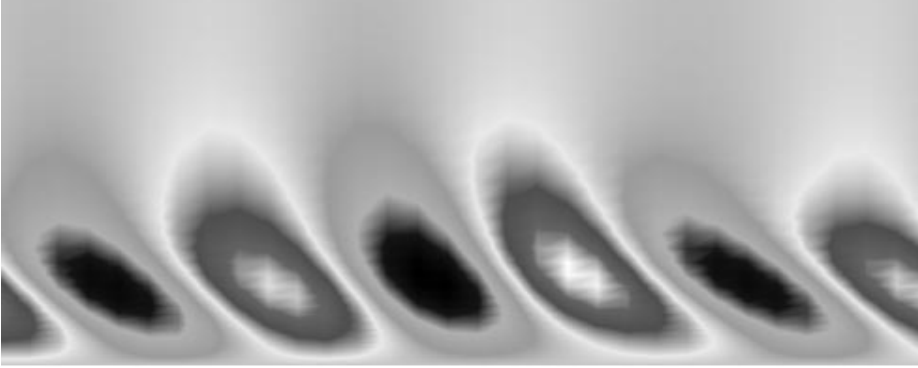
(c) $x_c = 0.45$

Figure 3. Spanwise planes of disturbance velocity (u) contours at chordwise locations for swept-wedge flow of SIM-I.
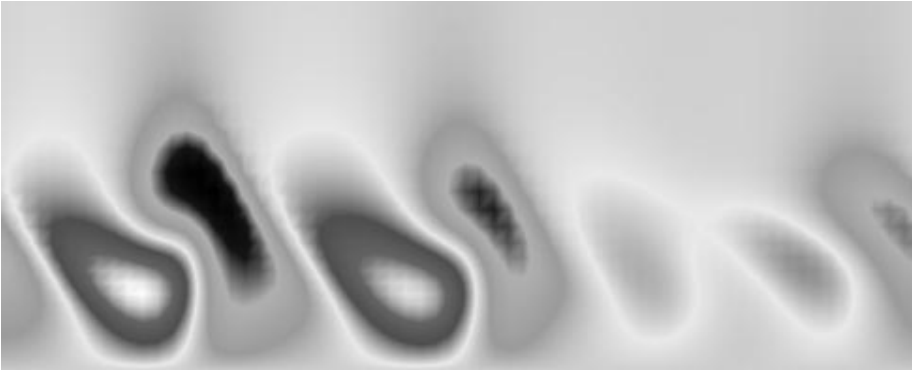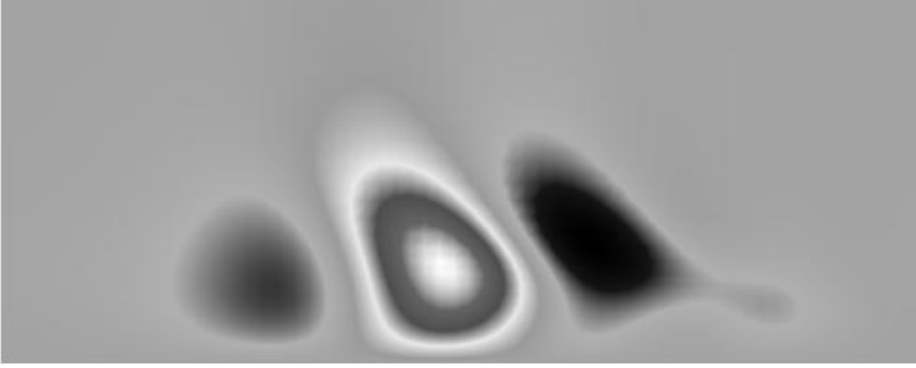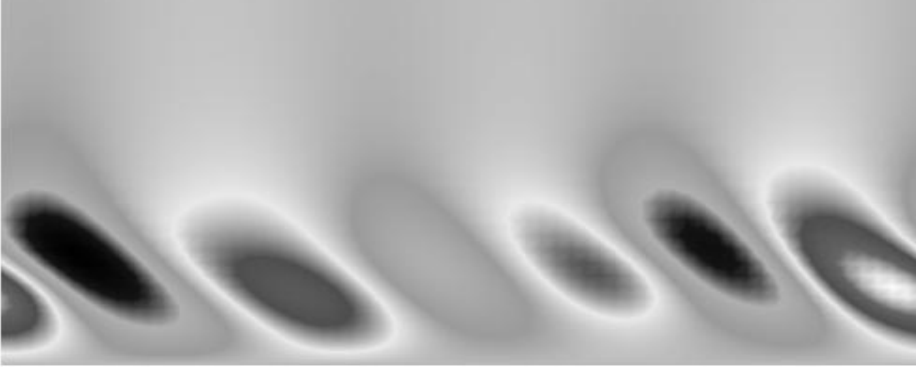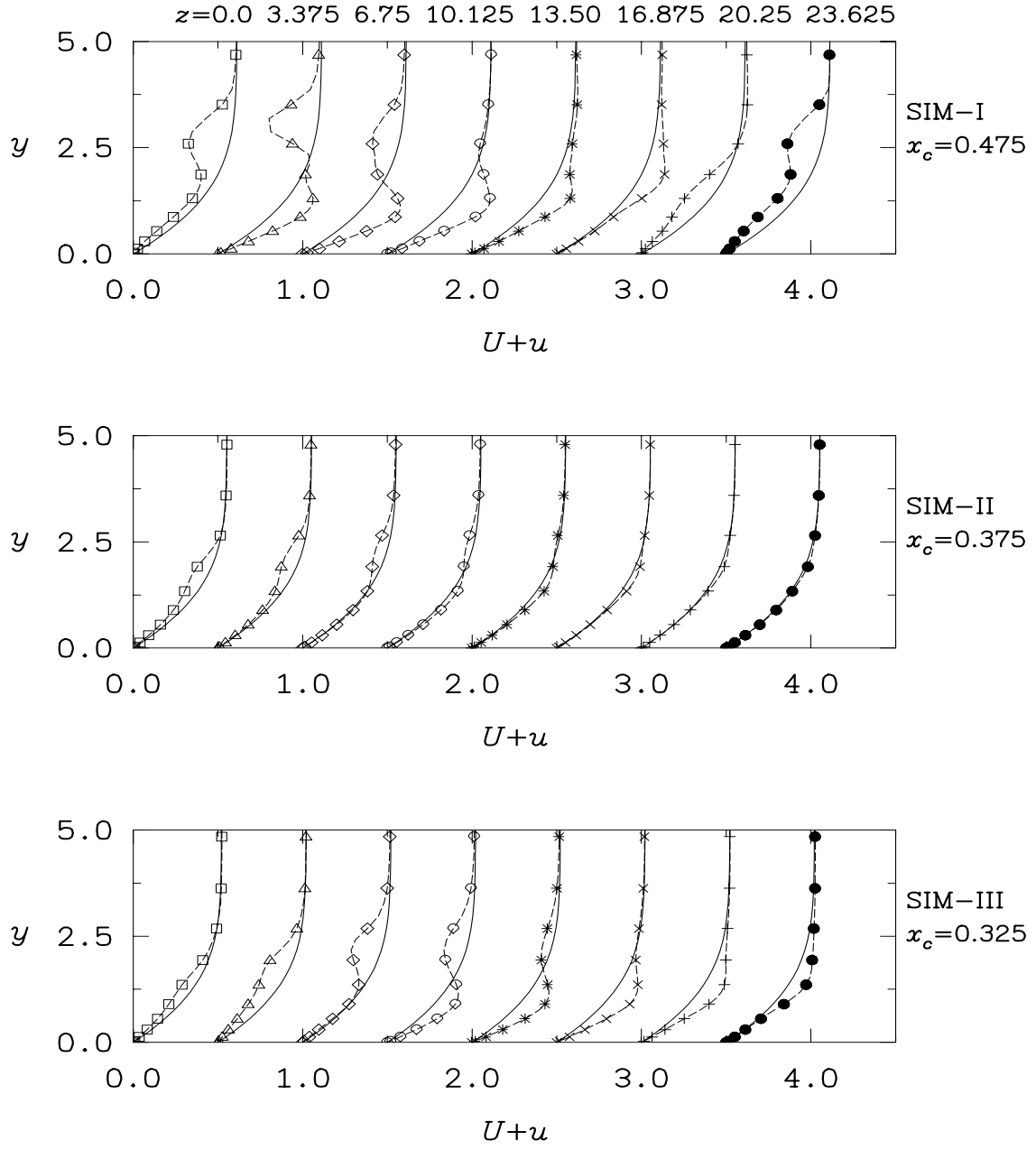
18
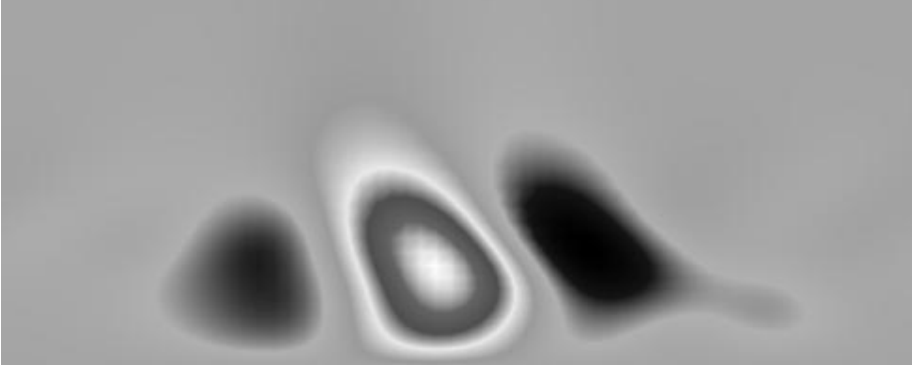
(a) $x_c = 0.25$

(b) $x_c = 0.325$
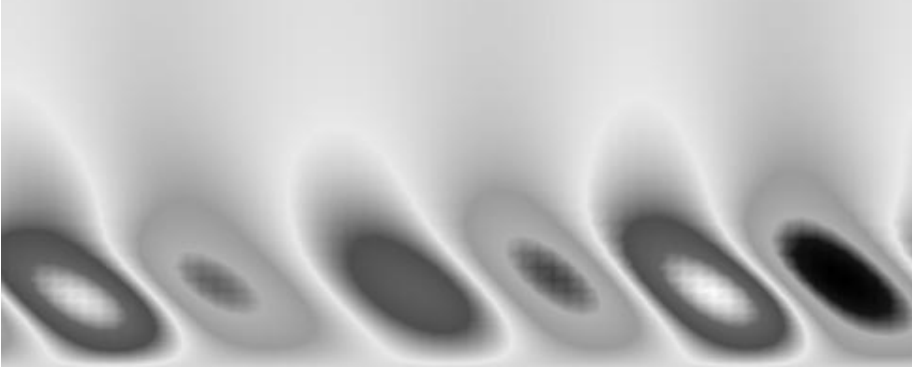
(c) $x_c = 0.375$

Figure 4. Spanwise planes of disturbance velocity (u) contours at chordwise locations for swept-wedge flow of SIM-II.

(a) $x_c = 0.25$

(b) $x_c = 0.30$

(c) $x_c = 0.34$

Figure 5. Spanwise planes of disturbance velocity (u) contours at chordwise locations for swept-wedge flow of SIM-III.

Figure 6. Chordwise (base + disturbance) velocity profiles at various chordwise and span-wise locations for swept-wedge flow.
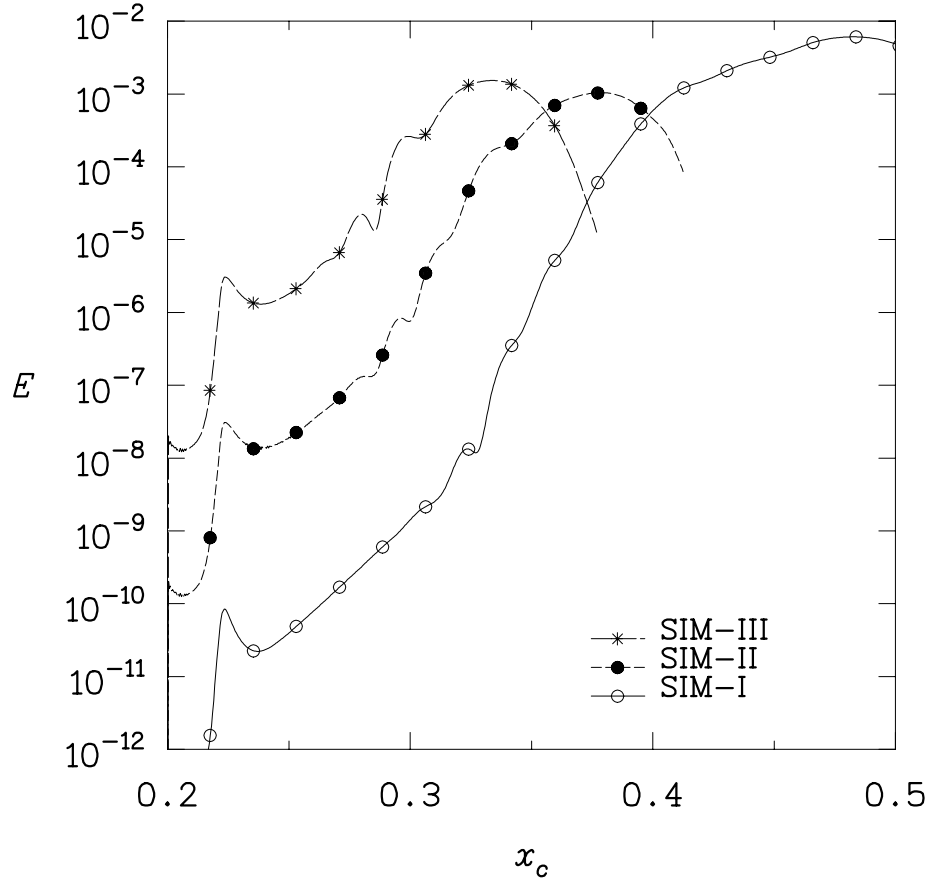
Figure 7. Energy of disturbance velocity with chordwise location for swept-wedge flow.
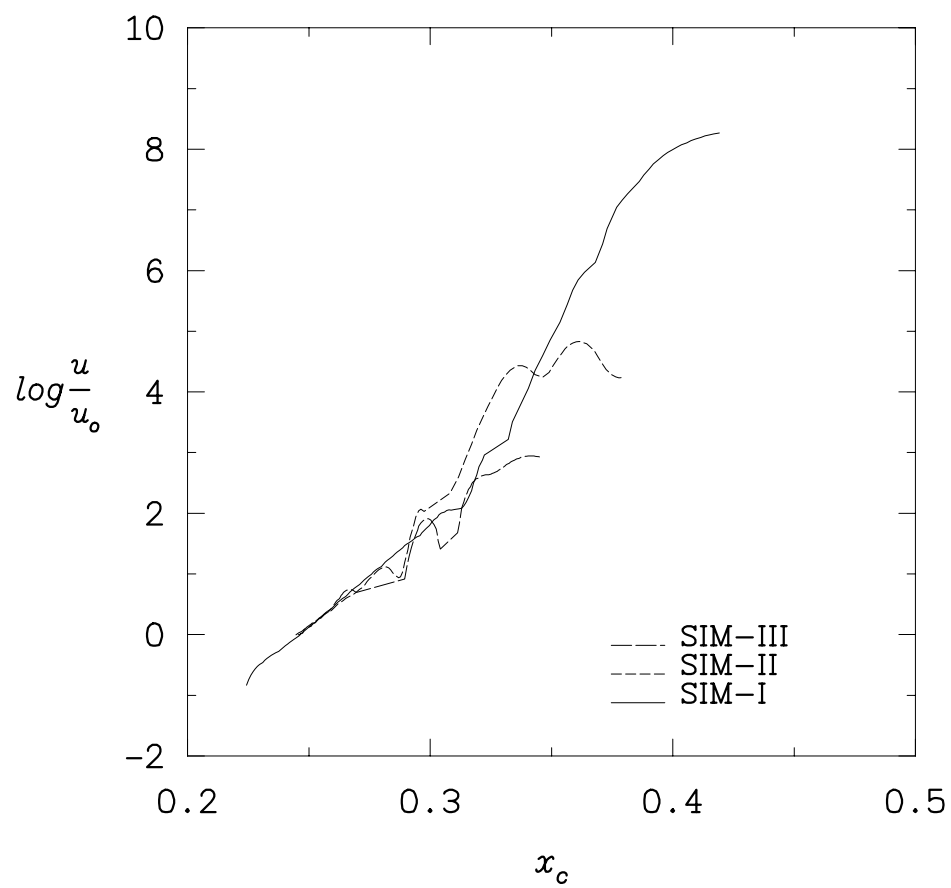
Figure 8. Estimation of N factor for swept-wedge flow.
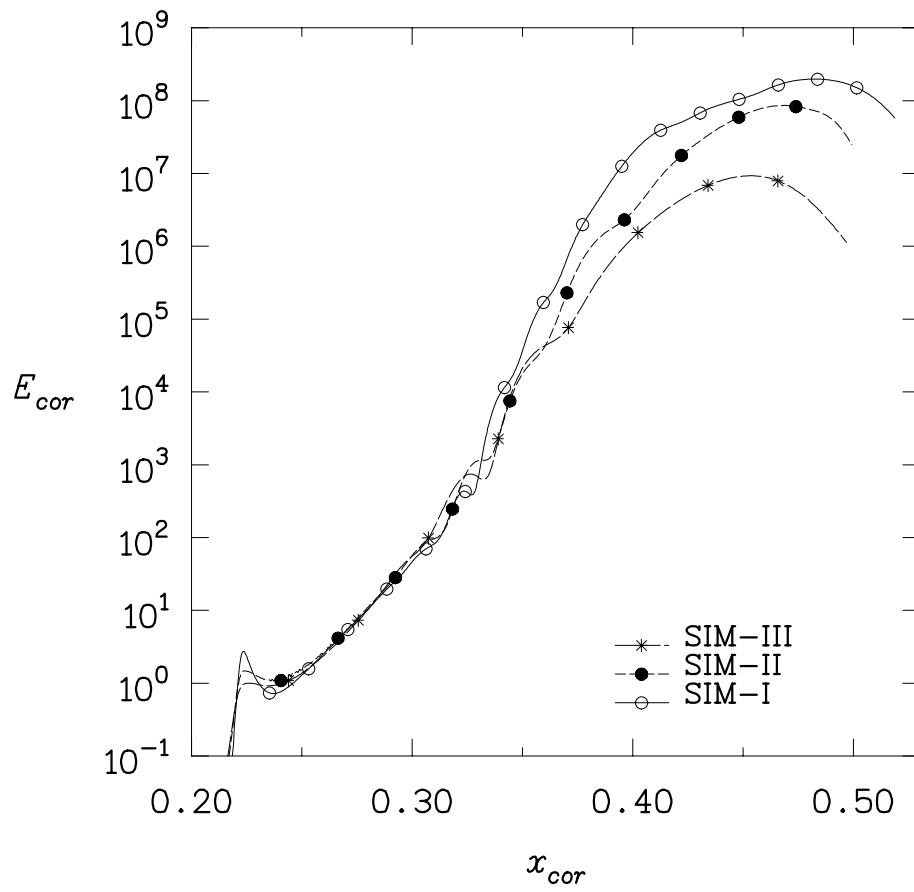
Figure 9. Correlated simulation results for crossflow instabilities in swept-wedge flow.
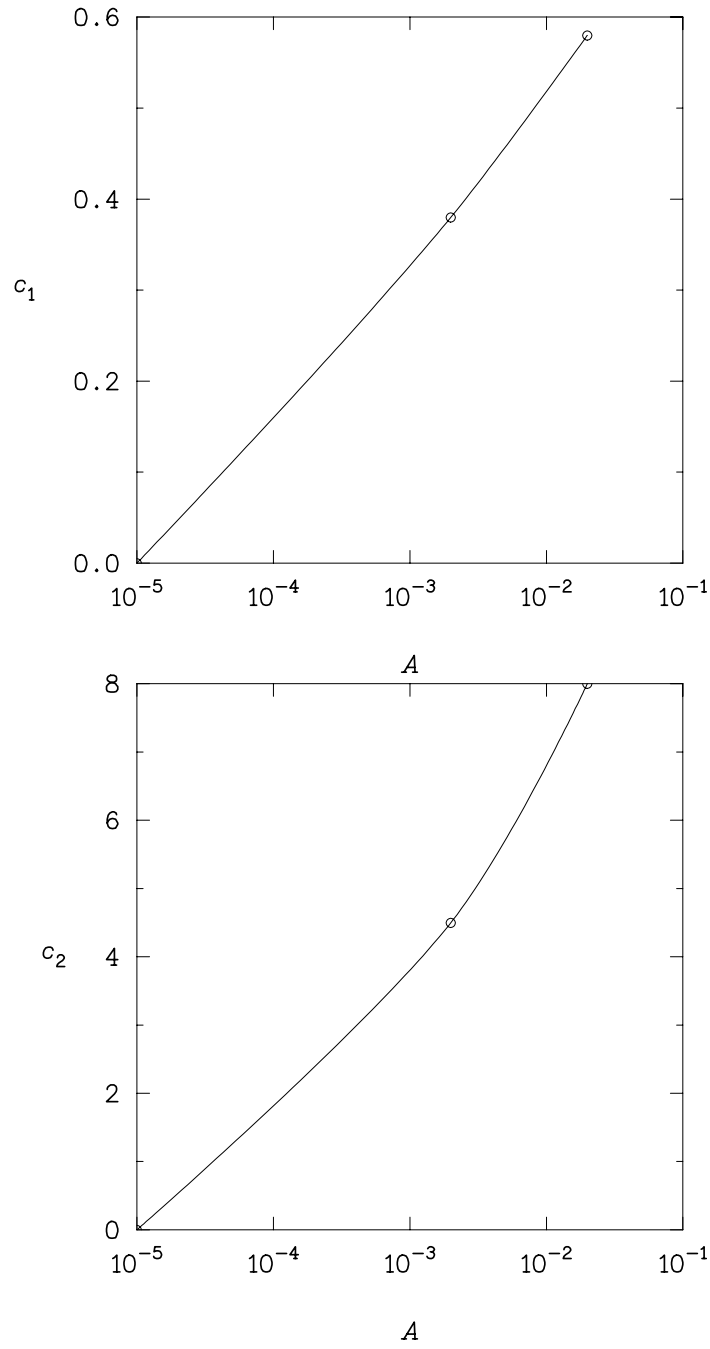
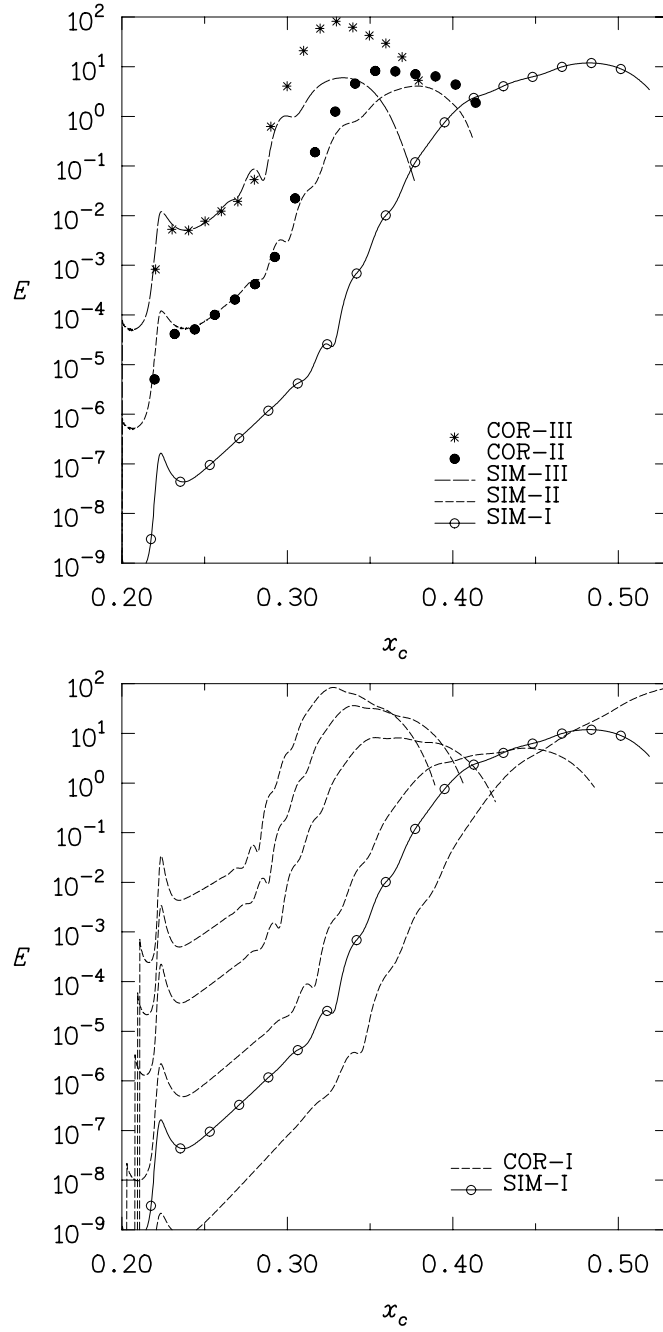Figure 10. Correlation coefficients with forcing amplitude for crossflow instabilities in swept-wedge flow.

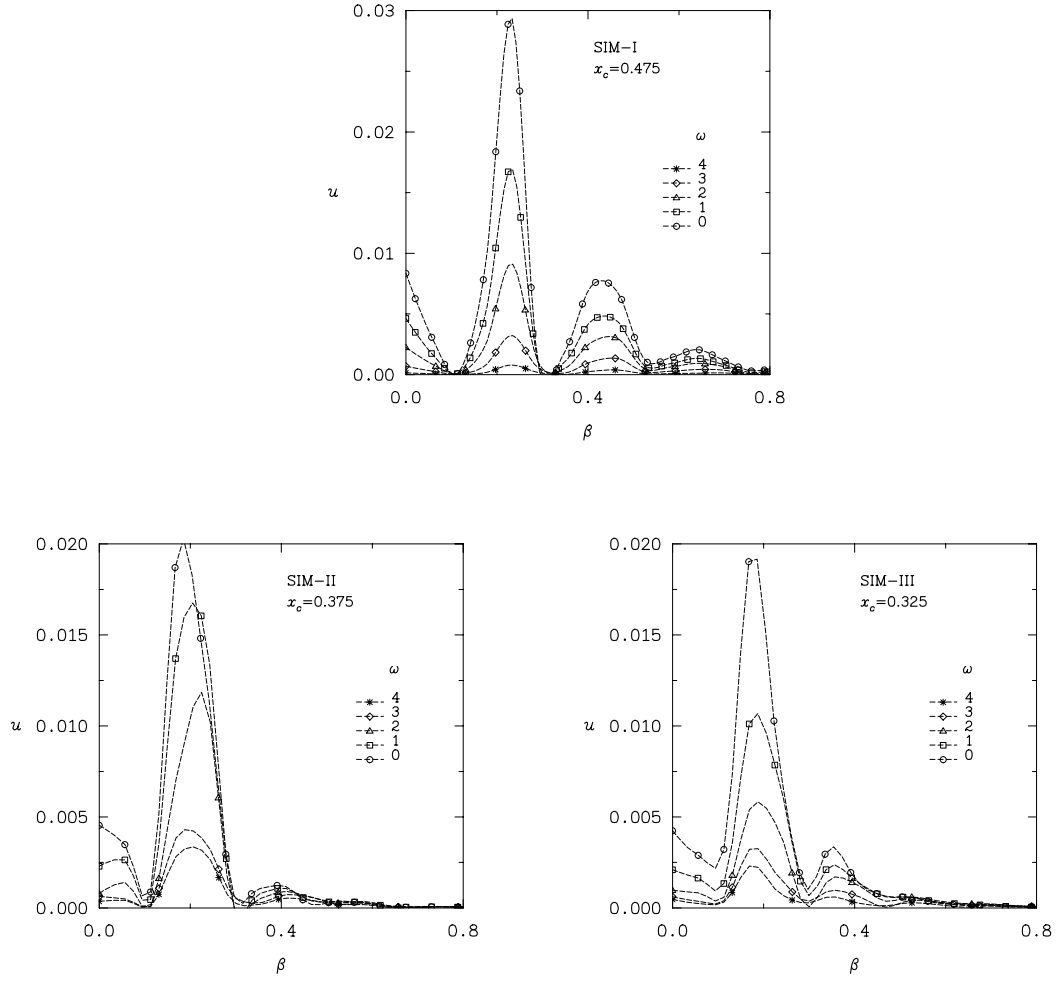Figure 11. Correlated and simulation results for crossflow instabilities in swept-wedge flow.

Figure 12. Chordwise velocity decomposed into spanwise wave-number components with frequency at various chordwise locations for swept-wedge flow.
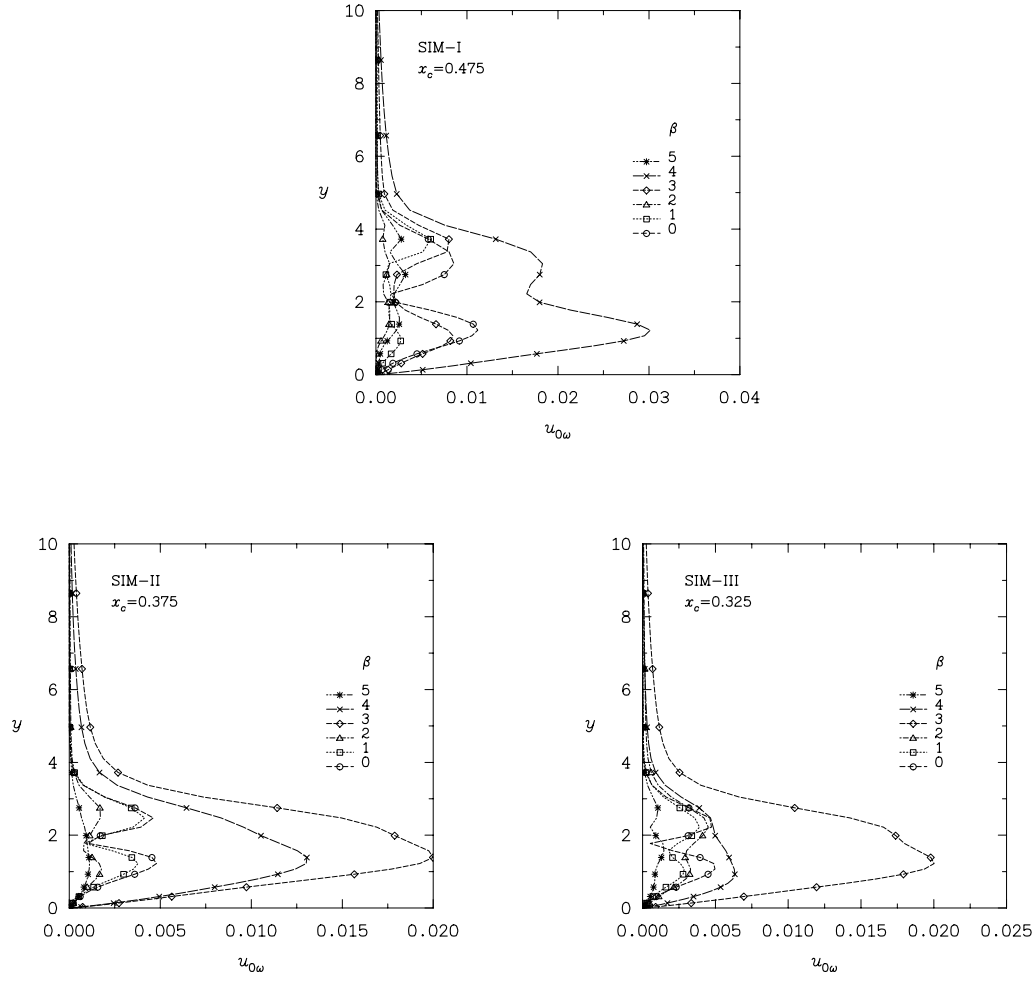
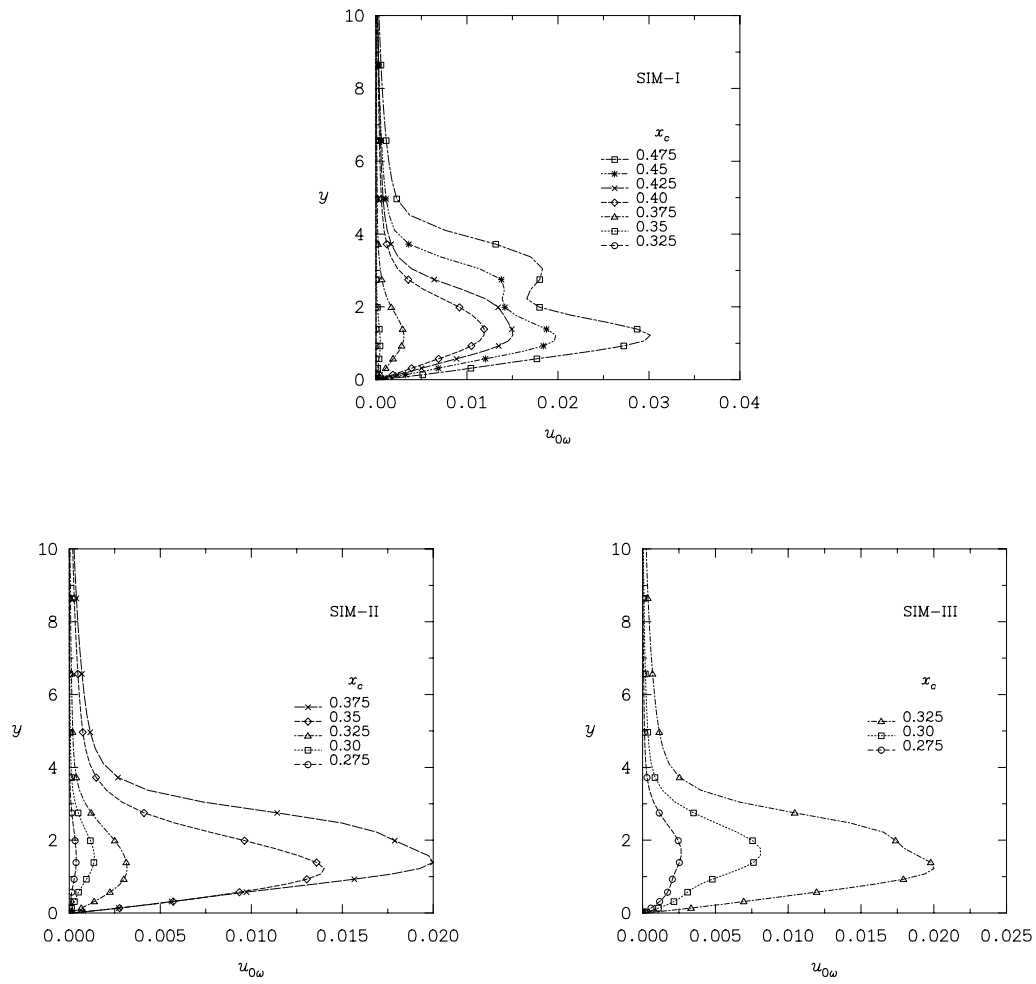Figure 13. Profiles of crossflow disturbance mode and spanwise harmonics.

Figure 14. Profiles of crossflow disturbance mode with chordwise distance.